

Spin Dynamics of a Magnetic Antivortex

Hao Wang and C. E. Campbell*

*School of Physics and Astronomy, University of Minnesota,
116 Church St. SE, Minneapolis, Minnesota 55455, USA*

(Dated: June 24, 2021)

We report on a study of the dynamics of a magnetic antivortex in a submicron, asteroid shaped, permalloy ferromagnet using micromagnetic simulations. As with vortex states in disk and square geometries, a gyrotropic mode was found in which a shifted antivortex core orbits about the center of the asteroid. Pulsed magnetic fields were used to generate azimuthal or radial spin wave modes, depending on the field orientation. The degeneracy of low frequency azimuthal mode frequencies is lifted by gyrotropic motion of the antivortex core, and restored by inserting a hole in the center of the particle to suppress this motion. We briefly compare the dynamics of the vortex state of the asteroid to the antivortex. The size dependence of the antivortex modes is reported.

PACS numbers: 75.75+a, 75.30.Ds, 75.40.Gb

Recently, there have been substantial efforts to understand the excitation spectrum of magnetic vortex structures.^{1,2,3,4,5,6,7,8,9,10,11,22,23} There exist two basic types of magnetic vortex structures in a quasi-two dimensional ferromagnet—a “circular vortex,” which we simply call a vortex in the remainder of this report, and an “antivortex”—both of which contain a nanometer scale core area where the magnetization is perpendicular to the plane of the sample.^{12,13} Cartoons of an antivortex and a vortex in an asteroid shaped particle are shown in Fig. 1. The winding number of an antivortex is -1 and $+1$ for a vortex. In addition to a fundamental interest in understanding the physics of these simple structures, the singular spin configurations in magnetic vortices and their dynamics suggest possible applications in spin logic operations.^{4,14,15} Much research has been done on a vortex in a circular disk, both theoretically and experimentally.^{2,3,5,6,7,9,10,11} Two classes of excitations in the circular disk have been identified. One is associated with the gyrotropic motion of the core about its equilibrium position with a frequency lower than 1 GHz for micron sized disks.^{2,3} The other type consists of spin wave modes at higher frequencies.^{5,6,7,9,10,11} The excitations of a vortex state in particles with a “cross” structure and in rectangular particles have also been observed; these differ from circular particles both because of the lower symmetry of the particle and because of the Landau domain structure around the vortex.^{1,3,4,8,22,23}

We are not aware of research on the dynamics of an antivortex, but such a study may be useful in understanding the dynamical properties of a complex multi-vortex structure such as in cross tie walls and in long particles.^{13,16,17,18,19} Since an antivortex has been found experimentally in an asteroid shaped permalloy particle (see Fig. 1),¹³ we focus on that system in this report.

We found that there is also a metastable vortex state at all sizes studied, shown in Fig. 1 (b), as well as two metastable or stable single domain states; the latter will not be discussed in this note. Both the vortex and antivortex states are sufficiently stable to sustain the weak perturbations that we applied without evolving into an-

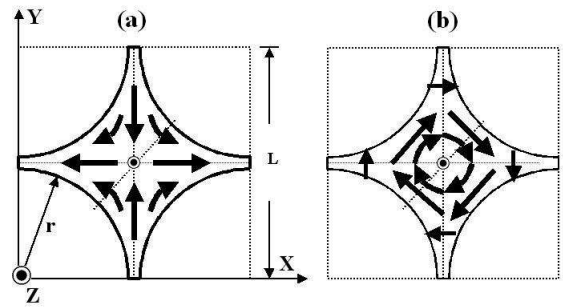


FIG. 1: Asteroid particles with a magnetic antivortex (a) and vortex (b). The solid arrows represent the direction of equilibrium magnetization inside the asteroid sample. The core region is indicated by the small circle about the center, and the dot at the center signifies a core pointing upward out of the plane.

other metastable state.

Considering the shape complexity of an asteroid, here we report only on micromagnetic simulations of the antivortex dynamics in this particle.²⁰ A gyrotropic mode was observed and two kinds of spin wave modes were excited by applying pulsed fields at different angles to the sample plane. The size dependence of the dynamic excitations was also systematically studied.

Asteroids were simulated with lateral size L ranging from 200 nm to 1 μm and thickness t ranging from 10 to 30 nm. The circular edges of the particles had a radius of $r = (96/200)L$. Typical permalloy material parameters were used, with saturation magnetization $M_s = 800$ emu/cc, exchange stiffness constant $A = 1.05$ $\mu\text{erg/cm}$, and gyromagnetic ratio $\gamma = 17.6$ MHz/Oe. For most simulations, a damping parameter of $\alpha = 0.04$ was used. The cell size for the discretized simulations was chosen to be 4 nm or 5 nm, which is shorter than the exchange length of 6 nm with the given material parameters.

Because of the out-of-plane magnetization of the antivortex core, one may expect that a gyrotropic mode will appear once the core is shifted away from its equilibrium

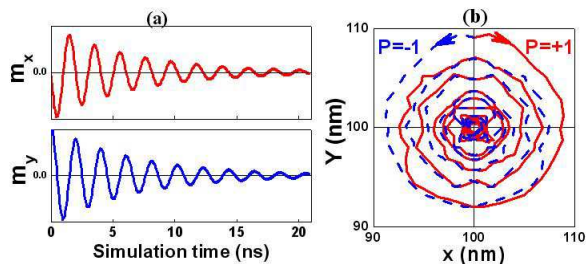


FIG. 2: (a) Time evolution of the x and y magnetization components in gyrotropic motion of an initially displaced core moving in remanence. (b) Trajectories of the antivortex core around its equilibrium position. The solid, clockwise helix is for core polarity $P = +1$, while the dashed, counter-clockwise path is for core $P = -1$. $L=200$ nm and $t=20$ nm.

position and released.² The core was shifted by applying a constant in-plane magnetic field. After the core stabilized at an off-center position, the applied field was removed. The remaining gyrotropic force on the antivortex core caused it to orbit about its equilibrium position, spiraling back to the center due to the damping. Fig. 2 shows the time evolution of the two in-plane components of the average magnetization and the trace of the antivortex core for a $200 \times 200 \times 20$ nm asteroid particle. The damped periodic behavior of the magnetization shows a gyrotropic mode with frequency 0.5 GHz. For an antivortex structure, the gyrotropic vector is proportional to the polarity of its core.² Therefore, changing the polarity of an antivortex core causes the gyrotropic orbit of the core to be in the opposite direction, as shown in Fig. 2(b), where $P = +1$ corresponds to the magnetization of core pointing up and $P = -1$ signifies pointing down.

Spin wave modes with higher frequencies may be excited by applying magnetic tipping pulse fields. We used Gaussian shaped pulses with a width of 30 ps and an amplitude of 5 Oe. To couple to a variety of spin waves, pulsed fields both in the plane of the particle and perpendicular to its plane were used. As one would expect from the additional torque exerted on the magnetic moments, in-plane pulses primarily activate spin wave modes with in-plane wave vectors curling around the center, i.e. azimuthal-like modes, while a perpendicular pulse couples most strongly to spin wave modes with the in-plane wave vectors along the radial direction, i.e. radial-like modes. Following the Fourier transform techniques of Ref. 9, we obtained a two-dimensional complex spectrum, with information about both the spectral amplitude and the spectral phase. The resonances in the power spectrum indicate eigenmode frequencies.

The power spectrum resulting from an in-plane pulsed field applied to a $500 \times 500 \times 20$ nm sample along \hat{x} direction is shown in Fig. 3 (a) for several cases. Of course, the spectra for the two oppositely polarized cores are identical. The low frequency resonance peak in the power spectrum of each of these corresponds to the core gyrotropic mode, while the resonances in the higher fre-

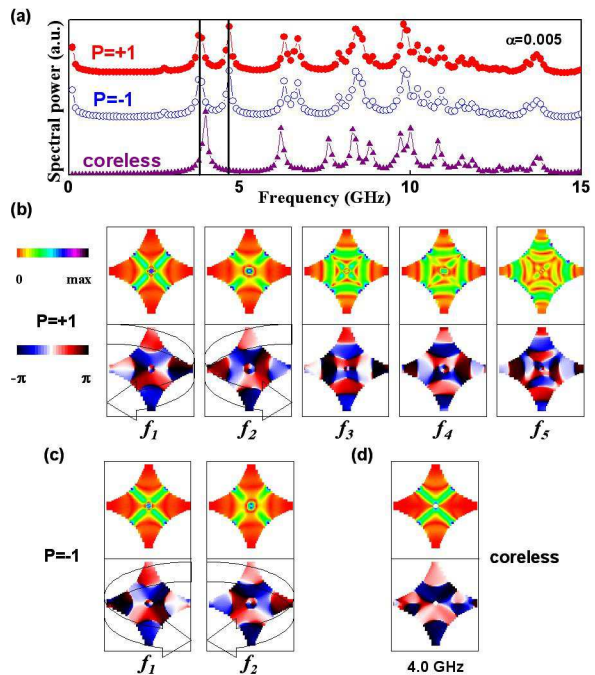


FIG. 3: (Color online) (a) Power spectra for $500 \times 500 \times 20$ nm asteroids in the antivortex state. The top pair are for asteroids with opposite antivortex core polarizations, labeled by P . The bottom spectrum is for an asteroid with a 20 nm hole at the center (coreless). (b) Spectral amplitude (top) and spectral phase (bottom) at resonance for the first five azimuthal spin wave modes in the $P = +1$ case at the resonant frequencies $f_1=3.8$ GHz, $f_2=4.7$ GHz, $f_3=6.3$ GHz, $f_4=6.7$ GHz and $f_5=8.4$ GHz of figure (a). (c) Spectral amplitude and phase images of the lowest two azimuthal modes at 3.8 GHz (left) and 4.7 GHz (right) for the $P = -1$ polarity. (d) Spectral amplitude and phase image of the lowest azimuthal mode at 4.0 GHz for the coreless asteroid. In (b) and (c), the chiralities of the two lowest modes with opposite polarizations are shown by the superimposed broad arrows.

quency region are spin wave modes that couple to the uniform pulse. The spectral details for each of the spin wave modes are shown in the Fig. 3(b) for the $P = +1$ case. The two lowest spin wave modes with frequencies of 3.8 GHz and 4.7 GHz are clearly azimuthal modes. They are mainly localized in an “X” shape region along the diagonal directions of the asteroid, where a spin wave well structure is formed due to the relative smallness of the internal field. The spectral phase of both modes continuously wraps through 2π around the azimuthal direction in the vicinity of the center of the asteroid but with opposite chiralities, indicating that these two modes are traveling waves with an angular mode number $|m| = 1$. The other excited spin wave modes with higher frequencies have weight distributed through the entire asteroid and their spectral phases show that they have a mixture of both azimuthal and radial characteristics.

One would expect the two lowest azimuthal modes to be degenerate if the antivortex core stays at the center,

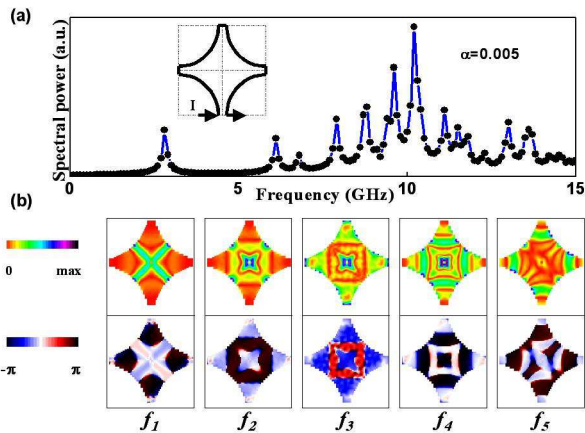


FIG. 4: (Color online) (a) Power spectrum for a 500x500x20 nm asteroid after excitation by an out-of-plane pulse field from a surrounding current. (b) Spectral amplitude (top) and spectral phase (bottom) at resonance for first five radial spin wave modes. Their frequencies are $f_1=2.8$ GHz, $f_2=6.1$ GHz, $f_3=6.8$ GHz, $f_4=7.9$ GHz, and $f_5=8.8$ GHz.

which is also suggested by the similarity of their spectral images. However, this degeneracy is lifted by the coupling between the azimuthal spin wave modes and the gyrotropic motion of the core, as was found in the vortex case.^{10,11} To further explore the relationship between this splitting and the core’s gyrotropic motion, we chose two 500x500x20 nm asteroids with different core polarities, the results of which were shown in Fig. 3. The two azimuthal modes for both core polarity cases appear at the same frequencies as in Fig. 3(a). However, the spectral phase images in Fig. 3(b) and (c) reveal a change of the ordering of the frequency of the two azimuthal modes. For $P = +1$ case in Fig. 3(b), the 3.8 GHz mode has a clockwise phase chirality while it is counter-clockwise for the $P = -1$ case. For comparison, we also simulated an asteroid of the same size but with a central hole of 20-nm diameter in order to remove the antivortex core.¹⁰ Only one resonance peak appears in the range of 3-5 GHz, as shown in the coreless spectrum in Fig. 3(a), at a frequency of 4.0 GHz. The spectral phase of this mode has one nodal line along the pulse field direction as shown in Fig. 3(d), indicating that the mode oscillates as a standing wave resulting from two degenerate azimuthal traveling wave modes with opposite phase chiralities.

An out-of-plane pulse field was applied to a 500x500x20 nm sample to excite radial spin wave modes, results of which are shown in the Fig. 4. Following the experimental setup in Ref. 8, the pulse simulated was that of an electric current loop around the asteroid sample as shown in the insert in Fig. 4(a). This pulse will not shift the antivortex core away from the center. Consequently, the resonances in the power spectrum in Fig 4(a) are predominantly radial modes and involve no coupling to the core’s gyrotropic motion. The spectral amplitude and phase of each spin wave mode exhibit a symmetry about

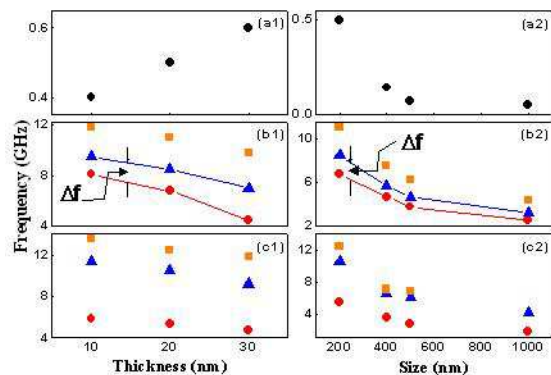


FIG. 5: Geometry dependence of dynamic modes of an antivortex in asteroid samples. The top row of pictures, (a1) and (a2), are results for the core gyrotropic modes. The middle row of pictures, (b1) and (b2) are results for the lowest three azimuthal spin wave modes. The bottom row of pictures, (c1) and (c2) are results for the lowest three radial spin wave modes. (a1), (b1) and (c1) are for asteroids with fixed size of 200 nm. (a2), (b2) and (c2) correspond to asteroids with fixed thickness of 20 nm. For spin wave modes, the different order of modes are distinguished by different symbols.

the origin as shown in the Fig. 4(b). The lowest radial mode is mainly distributed in the “X” shape region as in the azimuthal mode case. The spectral phase of the lowest mode exhibits nodes along the four long arms of the asteroid with the variation of the image color and brightness, while no nodes are along the four diagonal directions. The amplitudes of higher frequency radial modes are distributed over the entire asteroid and their phases show more nodes along both the diagonal and the arm directions of the asteroid.

The difference between the spectrum of the long arm direction and the diagonal direction of the asteroid can be ascribed to the different angles between the wave vector and the static equilibrium internal magnetic field. For radial modes, the wave vector is perpendicular to the internal field in the diagonal direction, thus having the characteristics of a Damon-Eshbach mode (DEM).²¹ However, along the long arm directions, the wave vector of radial modes is (anti)parallel to the internal field, which has magnetostatic backward volume mode (BVM) character.²¹ Thus, as a result of the unique spin configuration of a magnetic antivortex, both the azimuthal and the radial spin wave modes in the asteroid sample are hybrids of the DEM and BVM modes.

Fig. 5 shows the size dependence of the frequencies of the various modes obtained in our simulations. The frequency of the gyrotropic mode increases with the thickness of the asteroid but decreases with its area. Similar size dependence of the gyrotropic mode for a vortex in a circular disk has been found analytically.² Here, if we treat the asteroid sample topologically as a deformed circular disk, qualitatively we can understand the size-dependence of the gyrotropic mode in an antivortex

structure. The frequency of both azimuthal and radial spin wave modes decreases when either the thickness or the in-plane size of the asteroid increases. The drop of the frequency of spin wave modes can be explained by different mechanisms. On the one hand, an increase of just the in-plane size will effectively reduce the in-plane wave vector, with a consequent decrease of the frequency. On the other hand, an increase of just the thickness results in a lower static internal field while the in-plane wave vector remains the same. This lower static magnetic field will shift the dispersion curve to a lower frequency.²¹ Thus, for the same in-plane wave vector, i.e. the same mode, the frequency will decrease. Note also that the frequency difference between our two lowest azimuthal modes has the same trend as the gyrotropic mode. This qualitatively agrees with our previous argument about the coupling between the core's gyrotropic motion and the degenerate azimuthal modes since the resulting splitting of azimuthal mode degeneracy should be proportional to the frequency of the gyrotropic mode.

Finally we compare some of the antivortex results to the vortex states in the asteroid. We found that the gyrotropic frequency for the vortex state is approximately twice that of the anti-vortex state for the 200 nm asteroid, and four times as large for the 1 μm case. An important qualitative difference is that the chirality of the path of the antivortex core in gyrotropic motion is opposite to a vortex with the same core polarity. This will be significant for the low frequency dynamics of vortex/antivortex arrays. This feature is simply understood in terms of the Thiele equation for the gyrotropic motion of the vortex core, in which the gyrotropic vector is determined by a product of the core's polarity and its winding number.²

A comparison of the spin waves in these different systems is problematic. Here we note several features under-

lying this. Firstly, the symmetry group of the antivortex state of an asteroid is C_{2v} , while it is C_4 in the vortex asteroid, as it is in the vortex on a square.²² Thus the underlying symmetry classification of the spin wave states is significantly different. Secondly, the trade-off between exchange energy and dipolar energy is much more favorable to the formation of Landau domains in both the asteroid and square particle vortex states than in antivortex states.^{22,23,25} We find that the vortex state in the larger area asteroids contains well-defined triangular Landau domains with domain walls along the long axes of the asteroid, just as in the vortex state in square particles.^{8,22,23} Thus there should be well-defined intra-domain spin wave modes and localized domain wall modes in the large asteroid vortex state as found in the square vortex state. However, we did not find a tendency toward domains and domain walls in the antivortex state at any size. Consequently one expects to find the spin wave modes of the antivortex in asteroids more difficult to categorize than in these other cases.

In summary, we have studied dynamic excitations of a magnetic antivortex structure in asteroid samples and identified several eigenmodes of the system using micromagnetic simulations. The modes were generated by magnetic pulses similar to those likely to be used experimentally. The generation of lower symmetry modes would require field pulses of different spatial symmetry,^{22,23,24,25} which are not included here. The size dependence of the modes and the interaction between two different kind of modes have also been discussed. A brief comparison of these results to the dynamics of a vortex in asteroid and square particles is presented.

The authors gratefully acknowledge discussions with Professors Paul Crowell and E. D. Dahlberg. This work was supported in part by the Office of Naval Research under Grant No. ONR N/N00014-02-1-0815.

-
- * Electronic address: campbell@umn.edu
- ¹ B. E. Argyle, E. Terrenzio, and J. C. Slonczewski, *Phys. Rev. Lett.* **53**, 190 (1984).
 - ² K. Yu. Guslienko *et al.*, *J. Appl. Phys.* **91**, 8037 (2002).
 - ³ J. P. Park *et al.*, *Phys. Rev. B* **67**, 020403(R) (2003).
 - ⁴ S.-B. Choe *et al.*, *Science* **304**, 420 (2004).
 - ⁵ M. Buess *et al.*, *Phys. Rev. Lett.* **93**, 077207 (2004).
 - ⁶ R. Zivieri and F. Nizzoli, *Phys. Rev. B* **71**, 014411 (2005).
 - ⁷ B. A. Ivanov and C. E. Zaspel, *Phys. Rev. Lett.* **94**, 027205 (2005).
 - ⁸ K. Perzlmaier *et al.*, *Phys. Rev. Lett.* **94**, 057202 (2005).
 - ⁹ M. Buess *et al.*, *Phys. Rev. Lett.* **94**, 127205 (2005).
 - ¹⁰ X. Zhu *et al.*, *Phys. Rev. B* **71**, 180408(R) (2005).
 - ¹¹ J. P. Park and P. A. Crowell, *Phys. Rev. Lett.* **95**, 167201 (2005).
 - ¹² T. Shinjo *et al.*, *Science* **289**, 930 (2000).
 - ¹³ T. Shigeto *et al.*, *Appl. Phys. Lett.* **80**, 4190 (2002).
 - ¹⁴ Y. Gaididei *et al.*, *Phys. Rev. B* **61**, 9449 (2000).
 - ¹⁵ R. Höllinger, A. Killinger, and U. Krey, *J. Magn. Magn. Mater.* **261**, 178 (2003).
 - ¹⁶ K. L. Metlov, *Appl. Phys. Lett.* **79** (16), 2609 (2001).
 - ¹⁷ P. Eames, Ph. D thesis, University of Minnesota, 2004.
 - ¹⁸ P. Eames and E. D. Dahlberg (private communication).
 - ¹⁹ T. Okuno, K. Mibu, and T. Shinjo, *J. Appl. Phys.* **95**, 3612 (2004).
 - ²⁰ The LLG simulation code can be found at <http://llgmicro.home.mindspring.com>.
 - ²¹ B. A. Kalinikos and A. N. Slavin, *J. Phys. C* **19**, 7013 (1986).
 - ²² M. Yan *et al.*, *Phys. Rev. B* **73**, 014425 (2006).
 - ²³ M. Bolte, G. Meier, and C. Bayer, *Phys. Rev. B* **73**, 52406 (2006).
 - ²⁴ M. Yan *et al.* in *Condensed Matter Theories*, edited by J. W. Clark, R. M. Panoff, and H. C. Li (Nova Science Publications, New York, 2006), Vol. 20, p. 251.
 - ²⁵ M. Yan (private communication); Ph.D thesis, University of Minnesota, 2004.